Supplementary Materials for

Oligodendrocyte precursors migrate along vasculature in the developing nervous system

Hui-Hsin Tsai, Jianqin Niu, Roeben Munji, Dimitrios Davalos, Junlei Chang, Haijing Zhang, An-Chi Tien, Calvin J. Kuo, Jonah R. Chan, Richard Daneman, Stephen P. J. Fancy*

*Corresponding author. E-mail: stephen.fancy@ucsf.edu

Published 22 January 2016, *Science* **351**, 379 (2016)
DOI: 10.1126/science.aad3839

This PDF file includes:

Other Supplementary Material for this manuscript includes the following:
(available at www.sciencemag.org/content/351/6271/379/suppl/DC1)

Materials and Methods

Mice

Animal husbandry and procedures were performed according to UCSF guidelines under IACUC approved protocols.

Olig2-GFP

The Olig2-GFP reporter mouse is a generous gift from David Rowitch. To visualize Olig2+ cells in vivo, a knock-in allele of Olig2 was generated in which the 3' of the Olig2 gene is followed by IRES-GFP. The allele is termed Olig2-wt-IRES-GFP (Olig2-GFP).

Gpr124-/-

These mice are GPR124 null mice [25], lacking the orphan G protein–coupled receptor GPR124, which is essential for developmental vascular sprouting into forebrain and neural tube.

Cdh5cre/Gpr124-floxed

Embryonic tissue was used from these mice, which allow for endothelium-specific (Cdh5cre is vascular endothelium specific VE-Cadherin cre) deletion of the orphan G protein–coupled receptor GPR124 (GPR124-floxed).

PDGFRβ-/-

These mice are PDGFRβ (platelet-derived growth factor receptor β) null mice generated in the lab of P. Soriano. These mice completely lack pericytes in the CNS [36], and have been shown to be involved in BBB formation [26].

Olig2-tva-cre

A multi-functional mouse line was constructed previously [37] by inserting tva, an avian-specific retroviral receptor, and an IRES-cre recombinase cassette into the endogenous Olig2 locus by homologous recombination. This Olig2-cre allows for cre mediated activity in oligodendrocyte lineage cells.

APC-floxed

These mice have been described previously [28]. A conditional (floxed) allele of APC (adenomatous polyposis coli) provided by Dr. R. Fodde (Leiden University) [38]. Through intercrosses with an early Olig2 pan lineage cre-recombinase we can achieve conditional knockout of APC in OPCs.

Cxcr4-/-

These mice have been described previously [39].

Slice culture and time-lapse imaging

To label the shape of the vasculature we injected 6 μl of Rhodamine labeled BSL I (Vector Labs RL-1102) at 2mg/ml into the beating hearts of embryos dissected from the uterus and placed in room temperature PBS. Injection had a velocity of 15μl/minute

using a Syringe Pump (New Era Pump Systems NE-1000) and glass capillary bore of 2.3 micrometers. After 10 minutes allowing dye circulation, brains and spinal cords of embryos between E12 and E18 were dissected immediately in ice-cold artificial cerebrospinal fluid (ACSF; 125 mM NaCl, 2.5 mM KCl, 1 mM MgCl2, 0.4 mM ascorbic acid, 2 mM CaCl2, 1.25 mM NaH2PO4, 25 mM NaHCO3, 25 mM d-(+)-glucose, 2 mM sodium pyruvate, bubbled with 95% O2/5% CO2). Tissue was then embedded in 4% low melting point agarose in ACSF, and vibratome-sliced at 300 μm. Slices were transferred onto Millicell-CM slice culture inserts (Millipore) over culture medium (DMEM with 5% FBS, 1% N2 supplement, 4.5 g/L d-(+)-glucose, 1% penicillin, streptomycin and glutamine) in glass bottom 6-well plates and incubated at 37 °C, 5% CO2 for at least 2 hours. Cultures were changed with fresh medium containing 25mM HEPES before imaging. The plate was then transferred to an inverted Leica TCS SP5X confocal with an on-stage incubator (while streaming 5% CO2, 5% O2, balance N2 into the chamber), and imaged using a 10x immersion objective (NA=0.3) at specified interval and total imaging time in texts with intermittent repositioning of the focal planes. Maximum intensity projections of the collected stacks (~40 μm at 3-4 μm step size) were compiled in Imaris (Bitplane). For XAV939 treated slice cultures, postnatal day 1 (P1) cortical slice cultures were treated with 0.1 μM of the small molecule Wnt inhibitor XAV939 for 1 day in culture. Controls slices were DMSO (solvent for XAV939) controls.

Human developmental brain tissue

Pediatric brain specimens were immersed in 4% paraformaldehyde (PFA) for 2-3 days, and then stored in 0.5% PFA. The brains were examined by neuropathologists and subsequently cut into 1-cm plates coronally. Frontal-dorsal cortex was further dissected into 1 cm x 1 cm x 1 cm cubes and cryoprotected in 30% sucrose/PBS. Tissues were cut at 30μm thickness. Patients with non-neurological cause of death and no evidence of intracranial diseases are considered as controls. All specimens were collected with informed consent and in accordance with the University of California San Francisco (UCSF) Committee on Human Research.

Immunohistochemistry and Antibodies

The primary antibodies used were to the following proteins: PDGFRα (1:200, rat, 558774, BD Biosciences), PDGFRα (1:200, mouse anti-human, 556001, BD Biosciences), CD31 (1:200, rat, MEC13.3, BD Biosciences), CD31 (1:200, rabbit, ab28364, Abcam), CD31 (1:200, mouse anti-human, ab9498, Abcam), Olig2 (1:3000, rabbit polyclonal, C.D. Stiles, Harvard), Nkx2.2 (1:100, mouse monoclonal, Developmental Studies Hybridoma Bank), NG2 (1:200, rabbit, AB5320, Millipore), GFP (1:500, chicken polyclonal, GFP-1020, Aves Labs), PDGFRβ (1:200, rat monoclonal, 14-1402, eBioscience), Isl1/2 (1:200, mouse, 39.4D5, Developmental Studies Hybridoma Bank), BLBP (1:500, rabbit polyclonal, ABN14, Millipore), GLAST (1:200, rabbit, ab416, Abcam), Cleaved Caspase3 (1:200, rabbit monoclonal, 5A1E, Cell Signaling Technology), MBP (1:1000, rat, MCA409S, Serotec), Cxcr4 (1:200, rabbit, ab2074, Abcam) and SDF1 (1:200, mouse, 460-SD, RD Biosystems).

Expression profiling of Olig2-cre; DA-cat versus wild-type spinal cord at P4

Whole spinal cords were harvested, homogenized in Trizol and then RNA was extracted using RNeasy kit (Qiagen). Microarray analysis was performed at the Genetics Core Facility of the Gladstone Institute. For each of P4 wild-type and Olig2-cre/DA-cat, RNA from three animals was pooled for use in each array chip, and three Affymetrix Mouse Genome 430 2.0 chips were run for each group, for a total of nine animals for each group of wild type and Olig2-cre/DA-cat mice, as previously described [29]. Microarray data are available on the GEO website, GSE19403.

In vivo and ex vivo AMD3100 treatment

For in vivo treatment with AMD3100, mouse pups (wildtype and Olig2-cre:Apc(fl/fl)) were treated with AMD3100 by intraperitoneal injection at a concentration of 1mg/kg (or with no drug control sham) each day between the ages of P3 to P10, before euthanasia for further analysis. For ex vivo treatment with AMD3100, slice cultures of wildtype and Olig2-cre: Apc(fl/fl) mouse cortex and corpus callosum were prepared as described in above section (without the Rhodamine BSL injection), and then treated overnight with either AMD3100 (at 10μg/ml) or no treatment control, before fixation for further analysis.

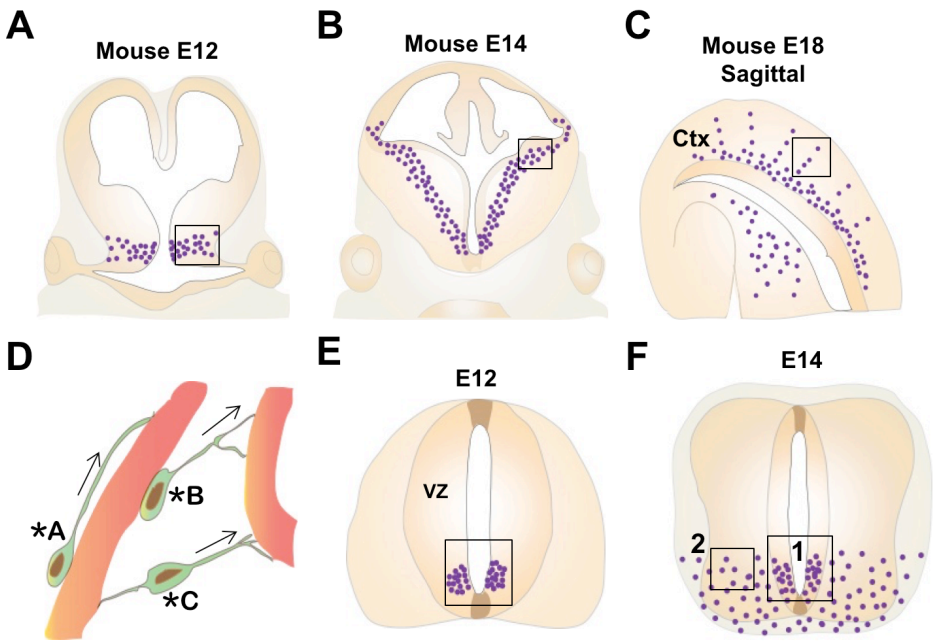

Fig. S1.

OPCs migrate extensively during development of the mouse brain and spinal cord from restricted ventricular zone progenitor domains. OPCs, which migrate more extensively than neurons and other glia, originate from restricted ventricular zone (VZ) progenitor domains [40] and migrate extensively to achieve uniform distribution in brain and spinal cord. (A) In the developing mouse forebrain, the first OPCs originate from ventral regions of the medial ganglionic eminence (MGE) at embryonic day 12. Migratory OPCs appear at E12 and then stream away from the MGE. Schematic to show OPCs (purple dots) first appearing from the ventral MGE in a coronal section of mouse brain. Images in main Fig. 1B-E are taken from area denoted by box. (B) Schematic showing migrating OPCs streaming dorsally from MGE to reach subpallial-to-pallial boundary at E14 in mouse coronal brain section. Images in main Fig. 1G-I are taken from area denoted by box. (C) The number of OPCs in the mouse cortex (Ctx) increases markedly between E16 and E18 as OPCs migrate outwards from deep to superficial cortical layers. Schematic of sagittal mouse cortex at E18 showing OPCs migrating from deep to superficial cortical layers. Images in main Fig. 1J are taken from area denoted by box. (D) We find that OPCs use vasculature as a physical scaffold for spatial migration during development. Schematic showing common OPC morphologies during migration, with cell body on abluminal vessel surface whilst extending a leading process along vessel (*A) or to another vessel (*B), or extending processes between more than one vessel (*C). (E) In mouse embryonic spinal cord, OPCs arise from a ventral domain of the ventricular zone called the pMN (motor neuron precursor domain), which gives rise first to motor neurons at E10.5 followed by OPCs at E12. Schematic to show first appearance of OPCs in the ventral pMN domain of the mouse spinal cord VZ at E12 (schematic shows transverse spinal cord). Images in main Fig. 2D-F are taken from area denoted by box. (F) Schematic to show spread of OPCs (purple dots) by E14 in the ventral half of the developing mouse spinal cord (schematic is transverse spinal cord). Images in main Fig. 2G and Fig. 2H are taken from areas denoted by box 1 and box 2 respectively.

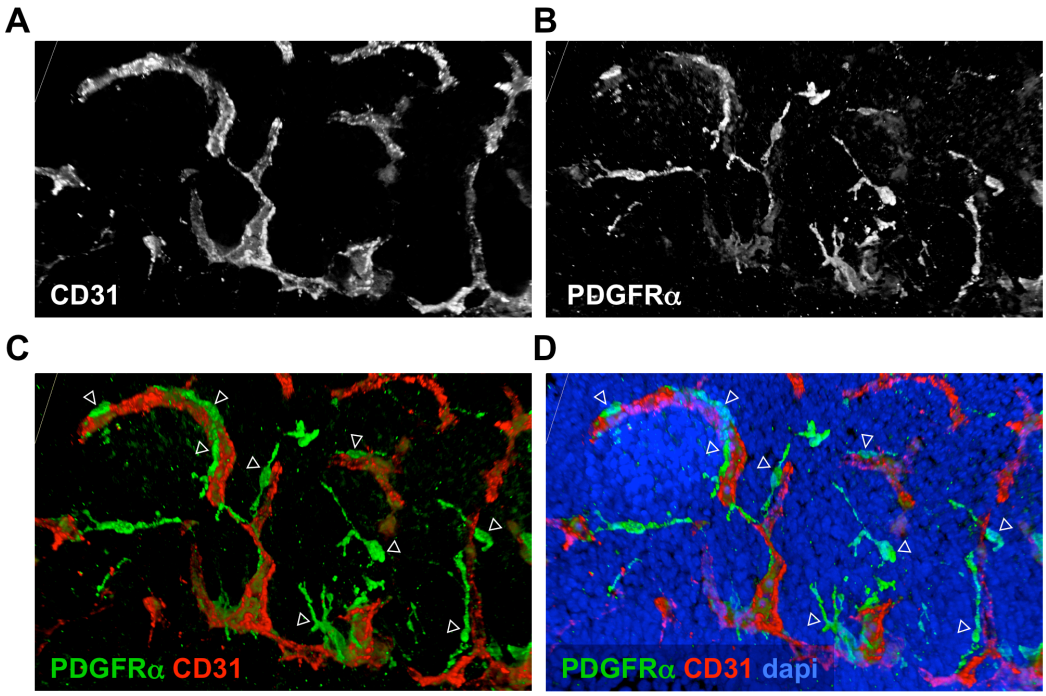

Fig. S2.

Migratory OPC association with vasculature on emergence from mouse E12 MGE. Migratory OPCs, defined by the expression of PDGFRα (B), first appear in the brain at E12 from the medial ganglionic eminence (MGE). Having left the MGE, they must find their way through dense tissue (D)(dapi labeling of cell nuclei), and show a marked association with, and elongation along, vasculature (labeled with CD31)(A, C).

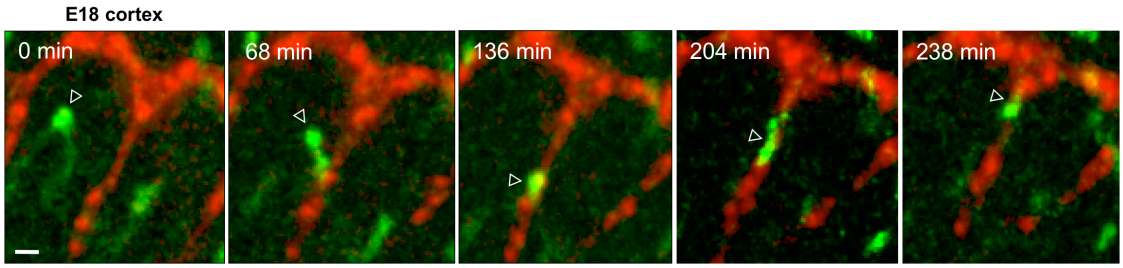

Fig. S3.

OPC 'crawling' directed motility on vessels. Time lapse imaging in a slice culture of embryonic cortex from Olig2-GFP reporter mice showing native GFP expression in green and vessels in red (labeled by intracardiac infusion with rhodamine labeled BSL I). A GFP-expressing OPC (arrowhead) engages a vessel, before demonstrating 'crawling' motility, elongating in the 204 minute panel to move along the vessel (Movie S2).

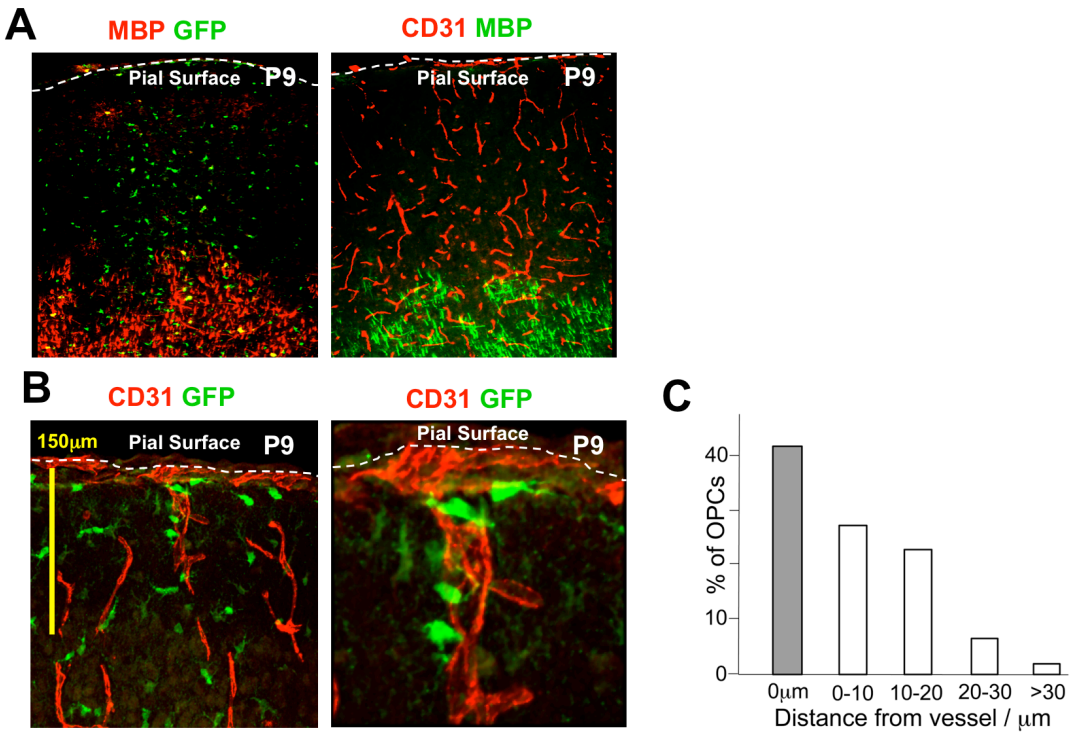

Fig. S4.
The association of OPCs with vasculature is not limited to early embryonic development, but is also observed at later times when OPCs are required to migrate. OPCs are highly associated with vasculature in the mouse early postnatal outer cortex. The mouse cortex continues to expand postnatally, with outer cortical layers remaining unmyelinated until several weeks after birth. OPCs generated postnatally from local cortex ventricular zone have a continuing need to migrate out in the expanding brain, and remain highly associated with vasculature in outer cortex at early postnatal times. (A) The outer cortex (near pial surface) of *Olig2-GFP* reporter mice remains unmyelinated (absence of Myelin basic protein MBP expression) at early postnatal times (postnatal day 9, P9), but contains numerous GFP-expressing OPCs. (B) GFP-expressing OPCs in the *Olig2-GFP* reporter mice remain closely associated with CD31-labelled blood vessels at P9 in the outer cortex. (C) Quantification of the proximity of GFP-expressing OPCs to vessels in the outer 150µm of the P9 cortex in *Olig2-GFP* reporter mice (n=4 animals). Over 40% of OPCs have their cell body directly on a vessel (0µm).

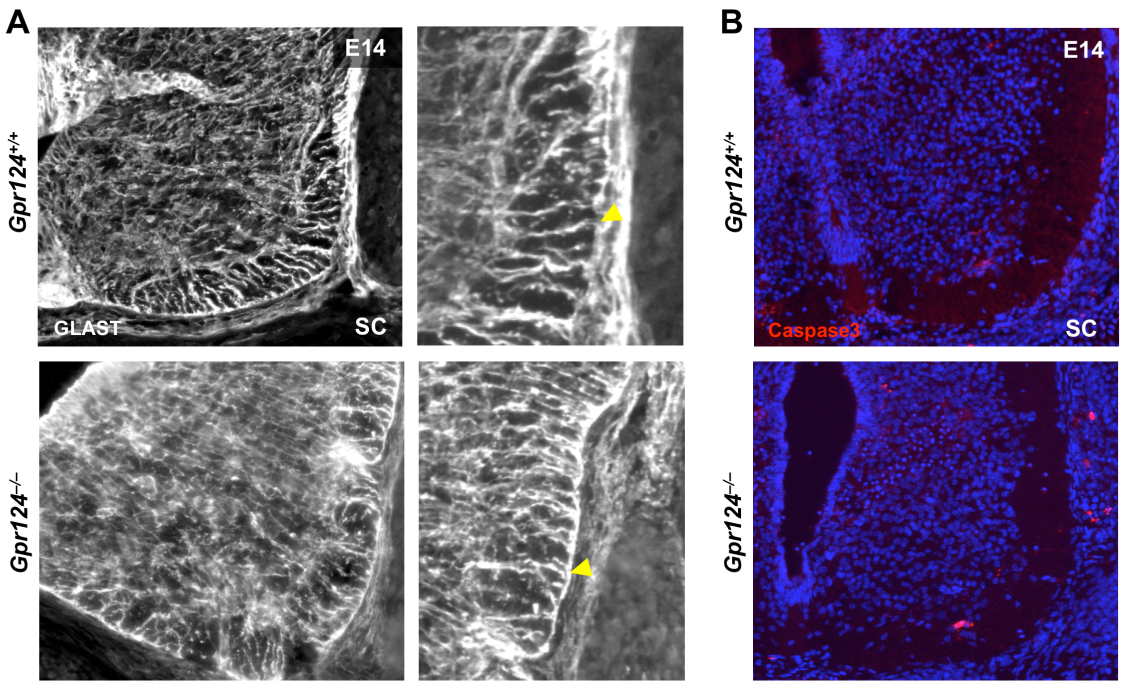

Fig. S5.
Characterization of embryonic spinal cord from GPR124 null mice for radial glial fiber integrity and cell death. (A) Glast staining for radial glial fibers shows intact fibers in the embryonic day 14 (E14) spinal cord of GPR124-/- null mice. (B) There is no increase in cell death (identified by the expression of Cleaved Caspase3) in the E14 spinal cord of GPR124-/- null mice compared to wildtype littermate controls.

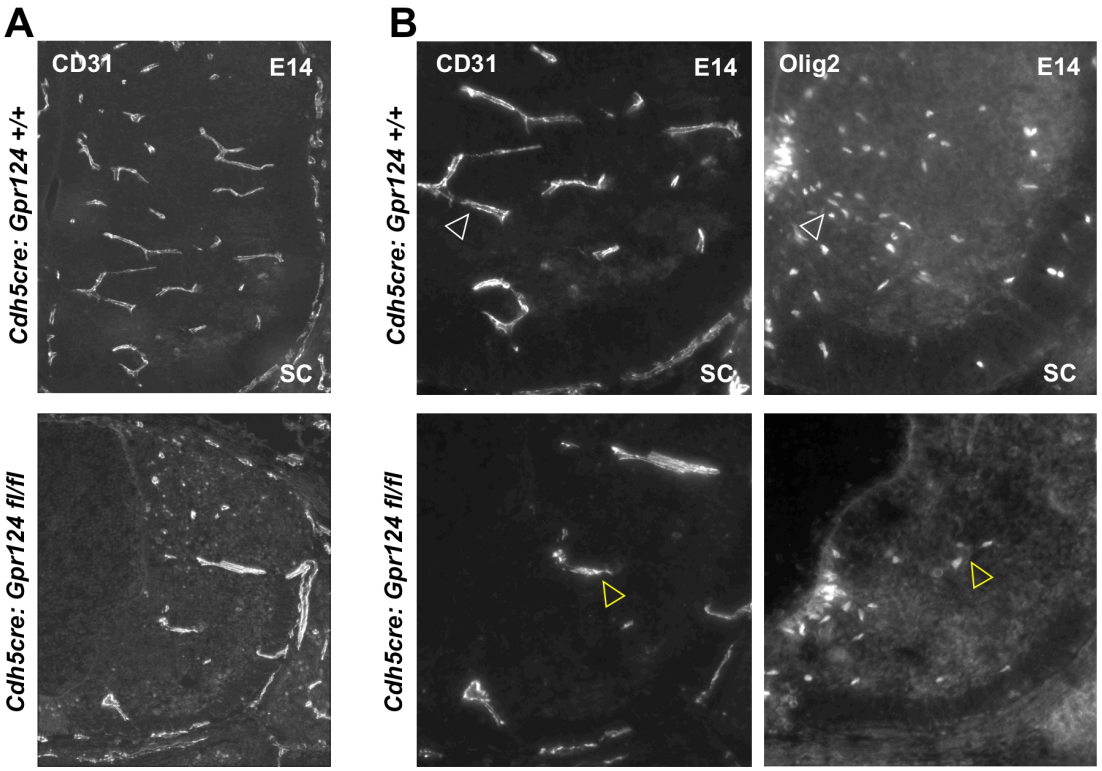

Fig. S6.
OPC migration is severely disrupted in Cdh5cre:Gpr124 floxed mice. A Cdh5cre line was used (Cdh5cre is a vascular endothelium specific VE-Cadherin cre) to conditionally ablate GPR124 from endothelial cells by crossing with a GPR124 floxed mouse. (A) These Cdh5cre:Gpr124 fl/fl mice have significant reductions in vasculature in the E14 spinal cord compared to wildtype (Cdh5cre:Gpr124+/+) littermates. (B) Serial 12μm sections of vasculature (CD31) and OPCs (Olig2) in ventral E14 spinal cord of wildtype Cdh5cre:Gpr124+/+ and Cdh5cre:Gpr124-floxed null mice. A severe deficit in Olig2 expressing OPC emigration into E14 ventral spinal cord is seen in mice in which GPR124 has been conditionally ablated from the vasculature using the Cdh5cre:Gpr124-floxed line, ruling out a cell intrinsic effect of Gpr124 loss in OPCs. Note that the few OPCs which do leave the pMN domain in Cdh5cre:Gpr124-floxed mice are in close proximity with the scant vessels which form in these mice (yellow arrowheads).

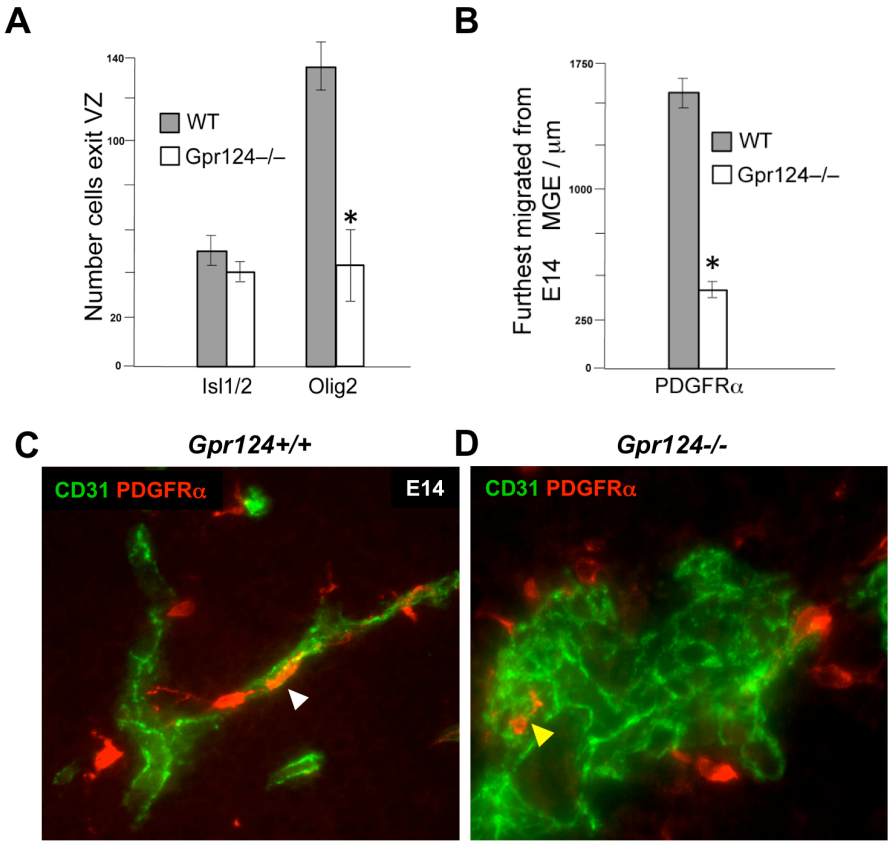

Fig. S7.

OPC migration in brain and spinal cord development of Gpr124 null mice is severely impaired. (A) OPC (expressing Olig2) emigration from the spinal cord ventricular zone (VZ) is severely disrupted in Gpr124 null mice whilst motor neuron (expressing Isl1/2) emigration is unaffected. Quantification of emigration from the pMN of Isl1/2+ motor neurons and Olig2+ OPCs in E14 Gpr124 null spinal cord and wildtype control littermates (n=4, t test *p= 7.3X 10-5). (B) OPCs expressing PDGFRα also show severe migration deficits in E14 brains of Gpr124 null mice, migrating only as far as the limits of the ventral vascular plexus. Quantification of furthest OPC distance migrated from the MGE in E14 WT versus Gpr124 null brains (n=4, t test *p=$7.8X10^{-8}$). (C) OPCs in E14 wildtype brains elongate along vessels during migration (white arrowhead), as previously described. (D) OPCs appear to accumulate around glomeruloid malformations in Gpr124 null embryonic brain (yellow arrowhead), trapped within the highly abnormal endothelial foldings (labeled with CD31).

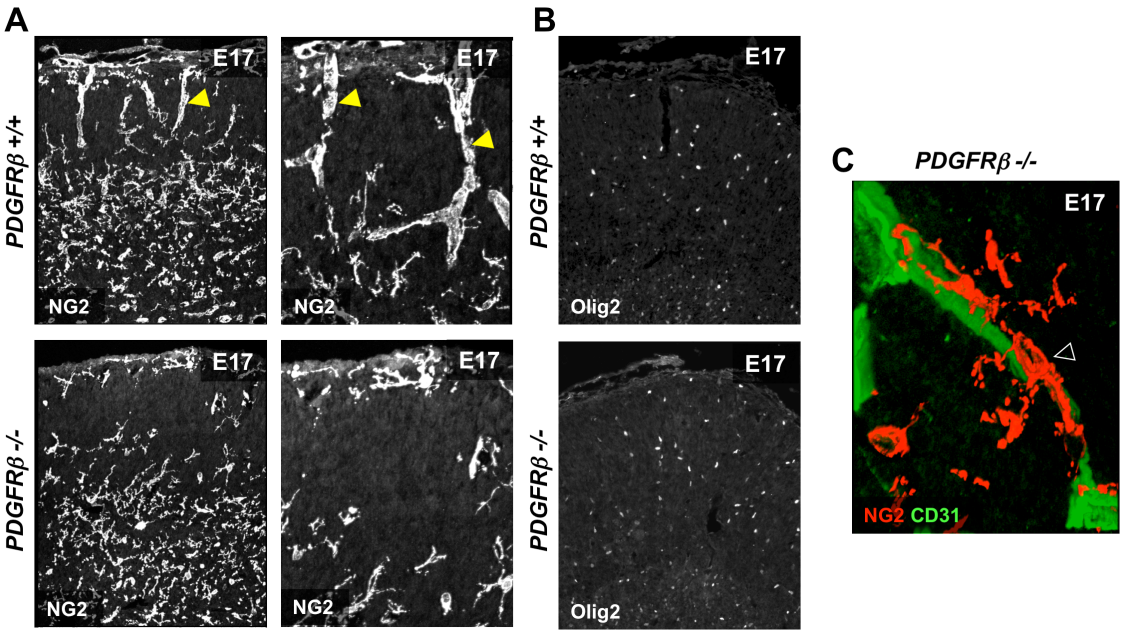

Fig. S8.
OPC developmental migration is normal in the absence of pericytes. (A) NG2 staining in wildtype PDGFRβ+/+ mice in embryonic day 17 (E17) cortex labels OPCs in addition to pericytes, and pericytes can be seen outlining vasculature (yellow arrowheads). In contrast, PDGFRβ-/- mice completely lack pericytes [26, 36], and NG2 staining labels only OPCs, with an absence of pericytes outlining vasculature. (B) OPC developmental migration is unaffected in pericyte deficient PDGFRβ-/- mice, with normal numbers of Olig2-expressing OPCs in the cortex at E17. (C) NG2 staining in cortex of PDGFRβ-/- pericyte deficient mice labels only OPCs, and highlights the intricate process association of OPC with CD31-labelled vasculature in the E17 cortex.

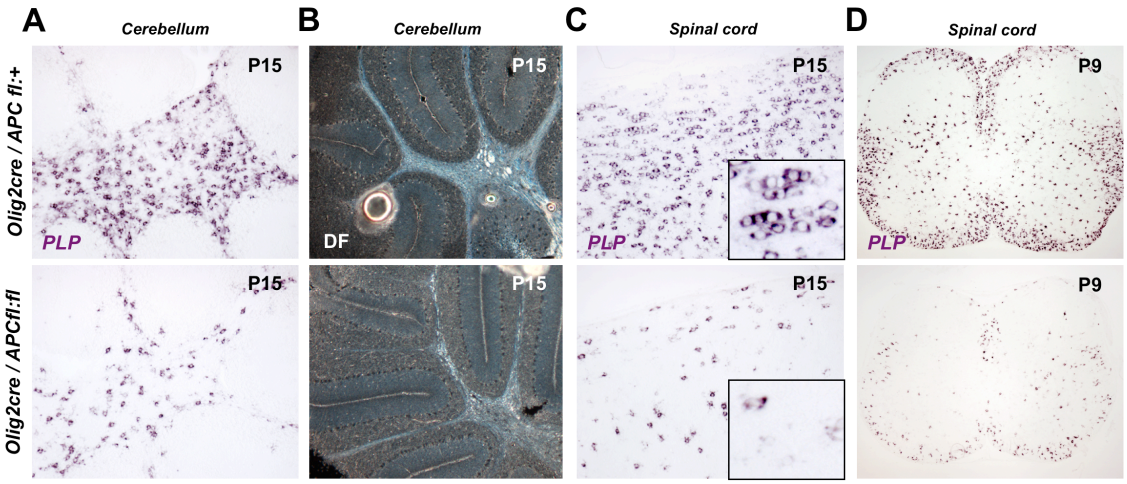

Fig. S9.
Loss of APC in OPCs causes significant deficits in developmental myelination. Generation of Olig2-cre:APC(fl/fl) mice results in ~85% efficiency of APC (adenomatous polyposis coli) protein loss in OPCs and ~15% "escapees" that fail to delete APC. (A) There is a significant reduction in the number of mature oligodendrocytes (expressing *PLP* mRNA) in P15 Olig2-cre:APC(fl/fl) developing cerebellar white matter (A), longitudinal cervical spinal cord (C), and P9 spinal cord (D), which leads to a severe hypomyelination as seen on dark field (DF) of P15 cerebellar white matter (B) compared to control Olig2-cre:APC(fl/+) littermates.

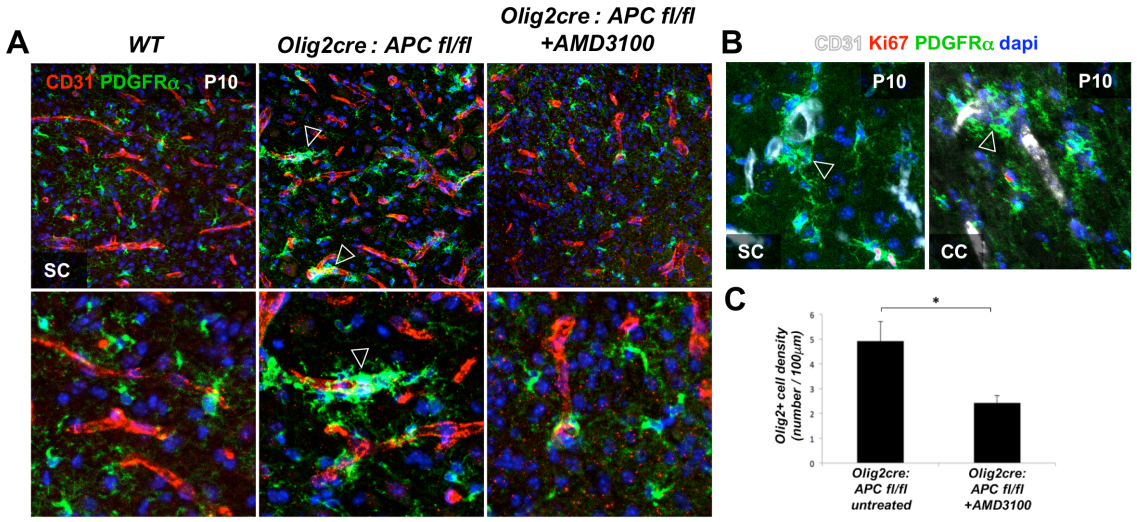

Fig. S10.

A Wnt-activated, Cxcr4-dependent mechanism drives attraction of OPCs to the vascular scaffold. (A) Aberrant accumulations of PDGFRα expressing OPCs can be seen around CD31-expressing vasculature in P10 spinal cord of Olig2-cre:Apc(fl/fl) mice (arrowheads in A) compared to wildtype (WT) mice. (B) This aggregation of OPCs around vessels does not represent an increase in OPC proliferation on the vessel itself, as evidenced by lack of Ki67 expression within the OPC clusters (arrowheads in B). (A) Treatment of Olig2-cre:Apc(fl/fl) mice in vivo with the Cxcr4/Sdf1 antagonist AMD3100 (+AMD3100) between developmental ages P3-P10 leads to a significant reversal of vessel-associated OPC clustering by P10 in the spinal cord (right panels in A). (C) Brain slice cultures of P10 Olig2-cre:Apc(fl/fl) corpus callosum have increased accumulation of Olig2 expressing OPCs around CD31-expressing vasculature. Treatment of Olig2-cre:Apc(fl/fl) slices ex vivo overnight with 10μg/ml of Cxcr4/Sdf1 antagonist AMD3100 leads to a reduction in vessel-associated OPCs compared to untreated. Graph shows number of Olig2+ cells on a vessel in P10 corpus callosum slice culture in untreated Olig2-cre:Apc(fl/fl) versus AMD3100 treated Olig2-cre:Apc(fl/fl) mice (*p= 0.012 Student T test). Counts are total number of Olig2 cells either on a vessel or closely associated with a vessel (within one nuclear diameter away from the vessel), expressed as number of Olig2 cells on each 100μm CD31 vessel segment.

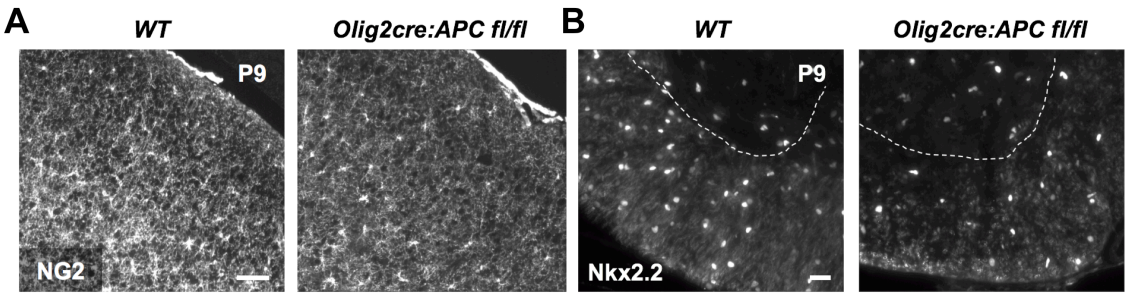

Fig. S11.
High Wnt tone in OPCs in Olig2-cre:Apc(fl/fl) mice leads to a general inability to disperse normally into CNS parenchyma. The increased attraction of OPCs to the vascular bed in Olig2-cre:Apc(fl/fl) mice reduces their ability to disperse normally to the most distant migratory destinations in the CNS, leading to reduced numbers in outer cortex (labeled with NG2 in A) and ventral funiculus spinal cord white matter (labeled with Nkx2.2 in B). Scale bar is 120μm (A), 25μm (B).

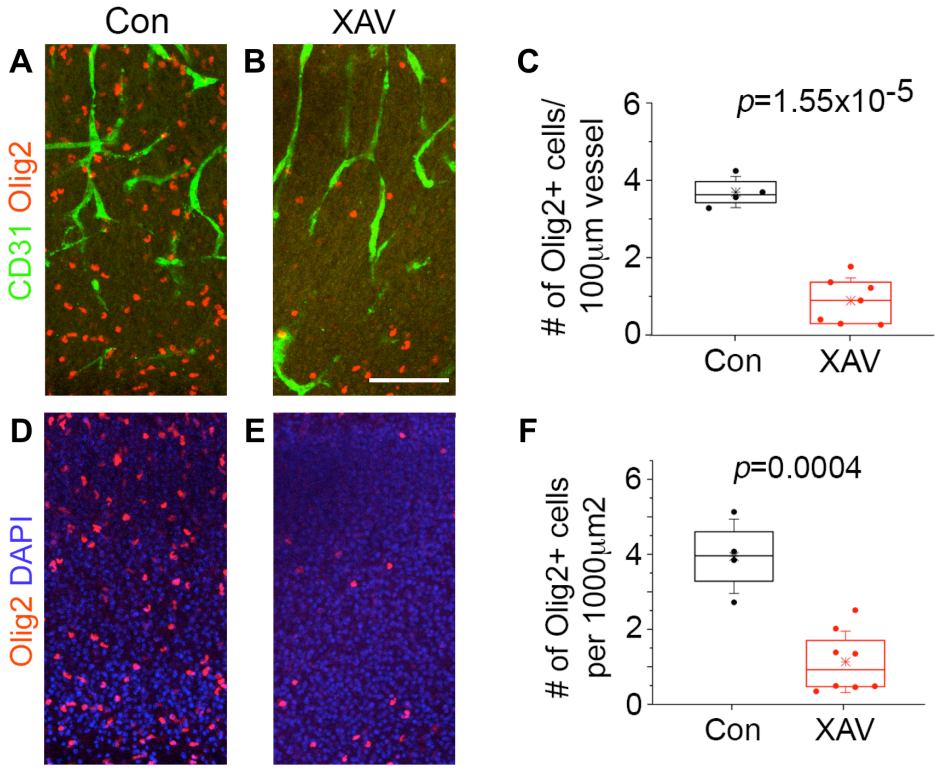

Fig. S12.

Loss of Wnt tone affects OPC recruitment to the microvasculature and migration. (A, B) Loss of Wnt tone in OPCs in postnatal day 1 (P1) cortical slice culture, when treated with 0.1 µM of the small molecule Wnt inhibitor XAV939 (XAV) for 1 day in culture, results in a significant reduction in the association of Olig2+ OPCs (red) with blood vessels (CD31, green) compared to untreated controls (Con). Scale bar=50 µm. (C) This significant reduction in association of OPCs with the microvasculature (p= 1.55 $X10^{-5}$) was quantified as number of Olig2 cells either on a vessel or closely associated with a vessel (within one nuclear diameter away from the vessel), expressed as number of cells on each 100µm CD31 vessel segment. (D, E) Loss of Wnt tone in OPCs in postnatal day 1 cortical slice culture, when treated with 0.1 µM of the small molecule Wnt inhibitor XAV939 for 1 day in culture, results in a reduced number (p= 0.0004) of Olig2+ OPCs migrating to reach the upper cortical layers (layers 2/3). (F) Quantification of Olig2+ cell numbers was done in layers 2 and 3. The box plots show 25 to 75 percentile with whiskers as 1-standard deviation. Asterisks mark the mean. Controls slices were DMSO (solvent for XAV939) controls.

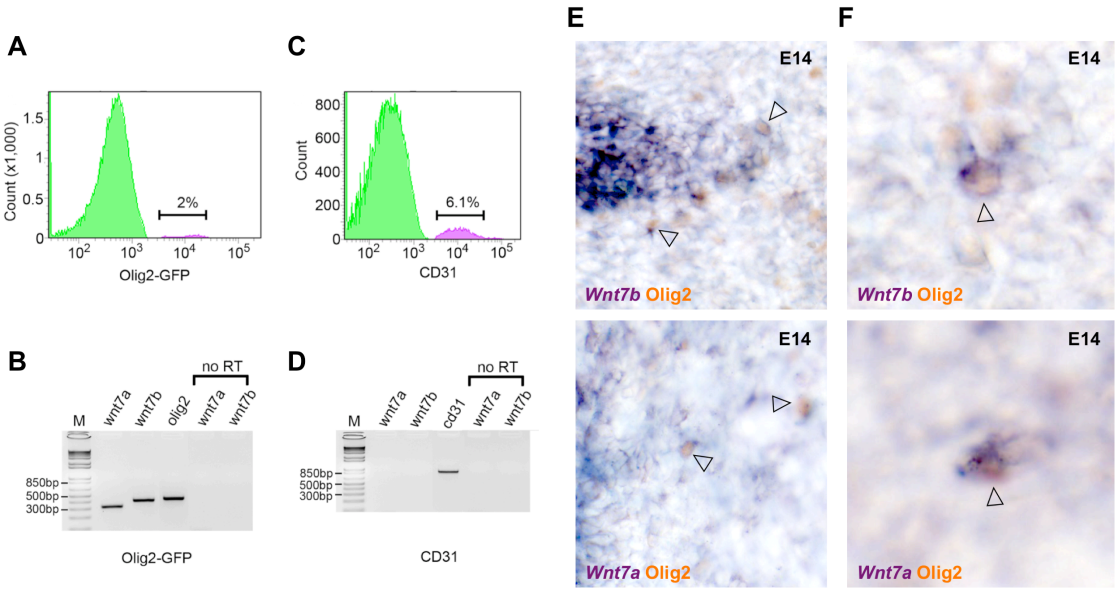

Fig. S13.

OPCs express Wnt7a and Wnt7b during their migration in the developing spinal cord and brain. (A) Olig2-GFP cells were sorted from E13 Olig2-GFP spinal cords by flow cytometry. Olig2-GFP cells collected for gene expression analysis were approximately 2% of the total live and single cell population. (B) Wnt7a and wnt7b were expressed by E13 Olig2-GFP OPCs by RT-PCR. (C) Cell suspension from E18 spinal cords were stained by anti-CD31 antibody. CD31+ cells were sorted by flow cytometry for gene expression analysis. CD31+ cells were about 6.1% of the total live and single cell population. (D) CD31+ endothelial cells showed no expression of wnt7a and wnt7b. By qRT-PCR, Olig2 was not expressed in the non Olig2-GFP and CD31+ populations. (E) Olig2+ cells can be seen expressing both Wnt7a and Wnt7b as they emerge from ventral forebrain ventricular zone germinal regions at E14 (arrowheads). (F) Olig2+ OPCs can be seen at a distance from their developmental MGE origin with maintained expression of both Wnt7a and Wnt7b in E14 ventral forebrain (arrowheads).

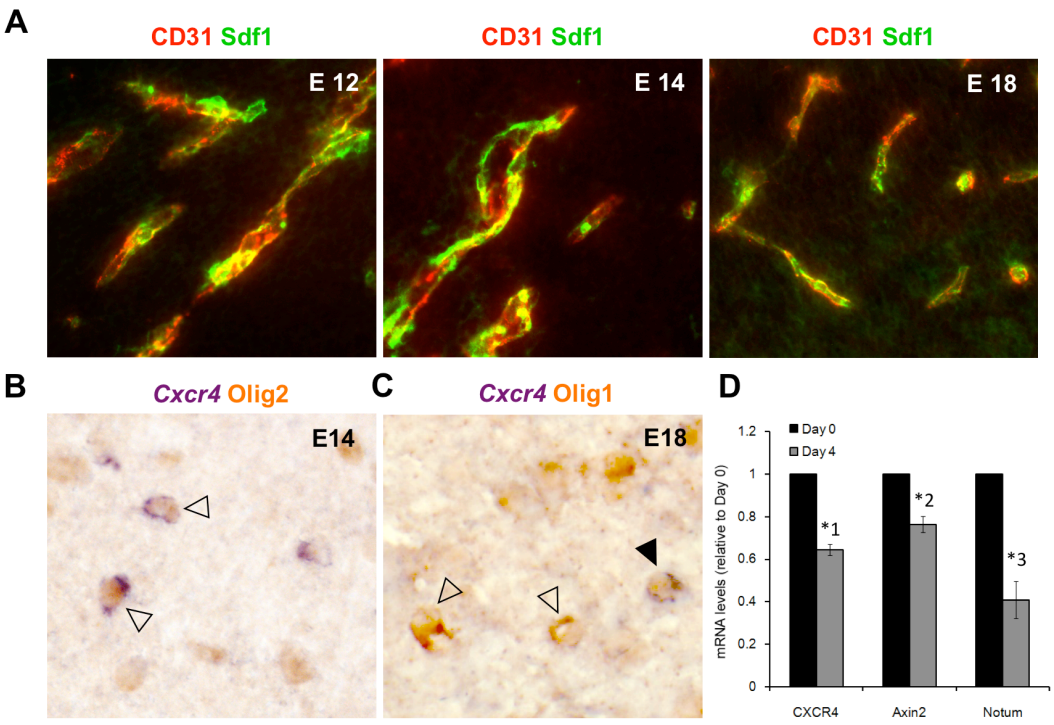

Fig. S14.

Cxcr4 and Sdf1 expression patterns in embryonic CNS. (A) Sdf1 expression is maintained throughout embryonic development of the ventral forebrain between E12 to E18, and seems to be expressed specifically by the endothelium (co-expression with CD31). (B) *Cxcr4* mRNA expression can be seen in Olig2 cells at E14 in ventral forebrain (unfilled arrowheads), a time when all Olig2 cells are OPCs. (C) At E18, Cxcr4 mRNA expression is seen in cells expressing nuclear Olig1 (OPCs)(filled arrowhead) but is downregulated in cells expressing cytomplasmic Olig1 (differentiating oligodendrocytes)(unfilled arrowheads). (D) Dissociated OPCs were cultured in vitro, switched to differentiation medium at Day 0, and allowed to differentiate for 4 days (Day 4) before RNA isolation. Quantitative RT-PCR shows that *Cxcr4* and the Wnt pathway (Wnt targets *Axin2* and *Notum*) are significantly downregulated upon OPC differentiation (*1 p= 5.24X10-4, *2 p= 0.0036, *3 p= 0.0022).

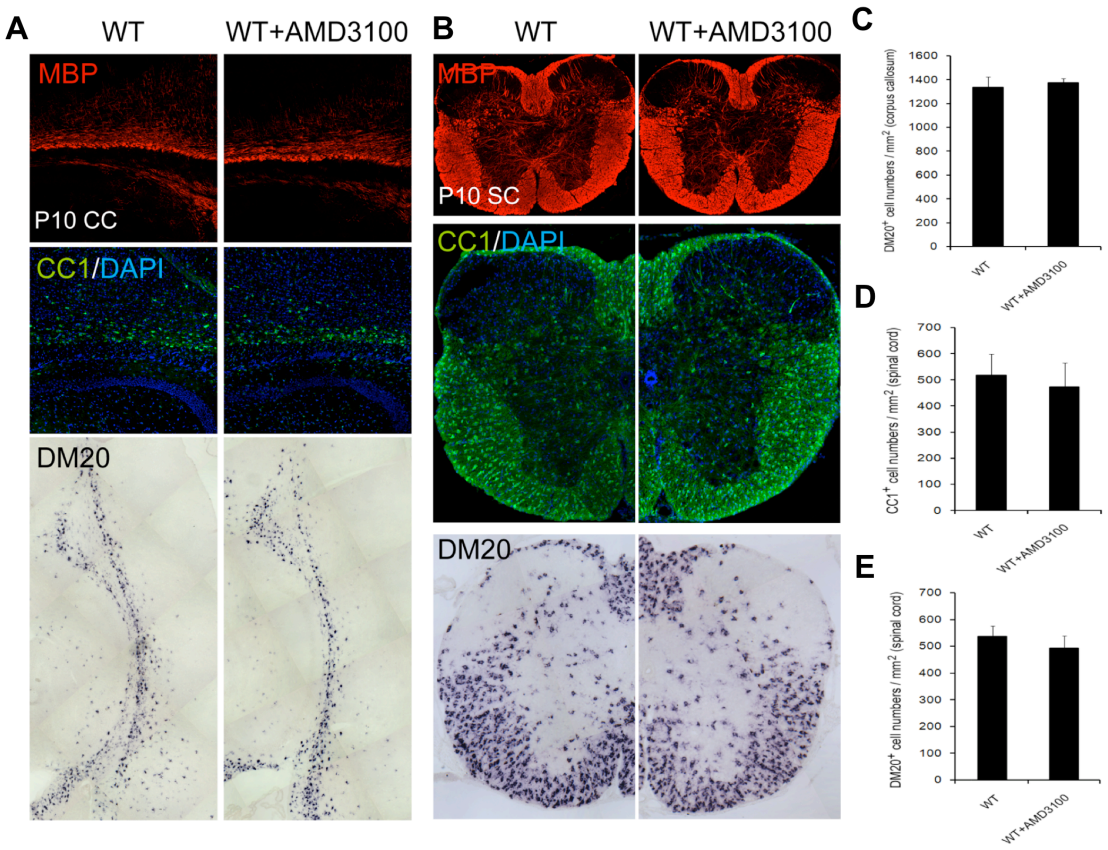

Fig. S15.
AMD3100 does not directly effect OPC maturation in wildtype mice. (A) Treatment of wildtype mice in vivo with the Cxcr4/Sdf1 antagonist AMD3100 (+AMD3100) between developmental ages P3-P10. Immunostaining for MBP (red), CC1 (green) and in situ-hybridization staining for *plp-DM20* in (A) P10 corpus callosum (CC) and (B) spinal cord (SC) showed no difference between wildtype (WT) untreated and WT treated with AMD3100 (WT+AMD3100) groups, suggesting that AMD3100 does not act directly on OPC differentiation. (C-E) There was no significant difference in the numbers of *plp-DM20*+ cells in corpus callosum (C) or spinal cord (E) or in numbers of CC1+ cells in spinal cord (D) between WT untreated and WT with AMD3100 (WT+AMD3100) at P10.

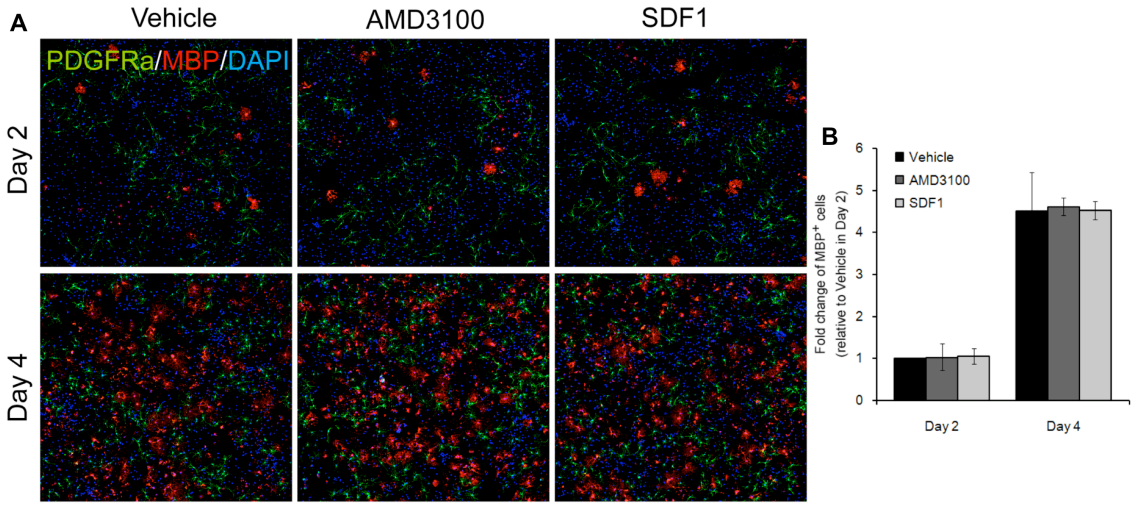

Fig. S16.
AMD3100 and SDF1 ligand do not directly effect OPC maturation in vitro. (A) Dissociated OPCs were cultured in vitro and were treated with either AMD3100 (10μg/ml), SDF1 (200ng/ml), or vehicle, for 2 and 4 days after switching to differentiation medium. PDGFRα (green) labels OPCs and MBP (red) labels mature oligodendrocytes. (B) There was no significant difference in the number of MBP positive cells in either treatment group compared to vehicle treatment at either 2 or 4 days (3 independent experiments at each time point), suggesting no direct effect on OPC differentiation. Cell counting was conducted on 6 randomly chosen fields under a 10× objective lens for each sample using an Image Pro Plus image analysis system. The MBP positive cell numbers in AMD3100 and SDF1 groups were compared to that in the Vehicle group at Day 2.

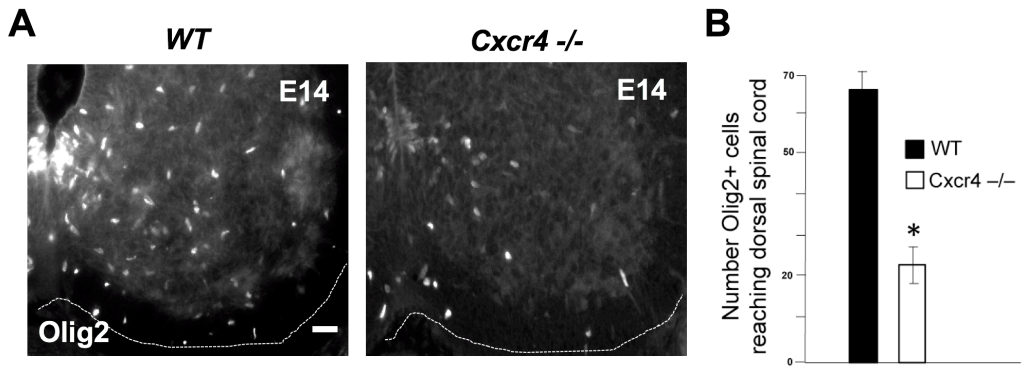

Fig. S17.
OPC migration is significantly impaired in mice lacking Cxcr4. (A, B) Reduced migratory ability of OPCs (labelled with Olig2) in Cxcr4 null mice spinal cord at E14 (A) with significantly reduced numbers reaching dorsal spinal cord at E14 (B) (*p= 0.001, T test, n=4). Scale bar is 25μm.

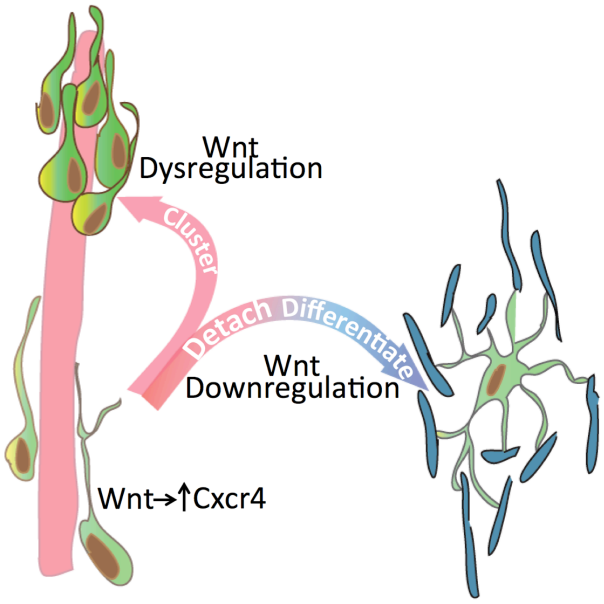

Fig. S18.
Wnt pathway links the timing of OPC migration and differentiation, with downregulation of Wnt required for both appropriate OPC detachment from endothelium and subsequent differentiation. This mechanism acts to prevent OPCs differentiating whilst associated with the vasculature during migration. Dysregulated high Wnt tone leads to both aberrant OPC clustering around vasculature as well as OPC differentiation block.

Movie S1
Time-lapse video in slice culture of embryonic cortex from *Olig2-GFP* reporter mice showing native GFP expression in green and vessels in red (labeled by intracardiac infusion with rhodamine labeled BSL I). A GFP-expressing OPC (green)(arrowhead) migrates along a penetrating vessel (red) in the E18 cortex. Each frame is at a 17 minute interval.

Movie S2
Time-lapse video in slice culture of embryonic cortex from *Olig2-GFP* reporter mice showing native GFP expression in green and vessels in red (labeled by intracardiac infusion with rhodamine labeled BSL I). An OPC, expressing GFP (green), in the mouse E18 cortex (arrowhead) first engages a penetrating vessel, before demonstrating 'crawling' or 'inchworm' motility, elongating the cell body to move further along the vessel. Each frame is at a 17 minute interval.

Movie S3
Time lapse imaging in slice culture of embryonic cortex from *Olig2-GFP* reporter mice showing native GFP expression in green and vessels in red (labeled by intracardiac infusion with rhodamine labeled BSL I). An OPC (green) in the E16 mouse cortex (arrowhead) demonstrates 'jumping' motility between vessels (red, outlined with dotted lines), extending a process to a parallel cortical penetrating vessel, before rapid movement of the cell body onto the new vessel. Each frame is at a 15 minute interval.

References and Notes

1. U. Fünfschilling, L. M. Supplie, D. Mahad, S. Boretius, A. S. Saab, J. Edgar, B. G. Brinkmann, C. M. Kassmann, I. D. Tzvetanova, W. Möbius, F. Diaz, D. Meijer, U. Suter, B. Hamprecht, M. W. Sereda, C. T. Moraes, J. Frahm, S. Goebbels, K. A. Nave, Glycolytic oligodendrocytes maintain myelin and long-term axonal integrity. *Nature* **485**, 517–521 (2012). Medline

2. Y. Lee, B. M. Morrison, Y. Li, S. Lengacher, M. H. Farah, P. N. Hoffman, Y. Liu, A. Tsingalia, L. Jin, P. W. Zhang, L. Pellerin, P. J. Magistretti, J. D. Rothstein, Oligodendroglia metabolically support axons and contribute to neurodegeneration. *Nature* **487**, 443–448 (2012). Medline doi:10.1038/nature11314

3. Q. R. Lu, T. Sun, Z. Zhu, N. Ma, M. Garcia, C. D. Stiles, D. H. Rowitch, Common developmental requirement for Olig function indicates a motor neuron/oligodendrocyte connection. *Cell* **109**, 75–86 (2002). Medline doi:10.1016/S0092-8674(02)00678-5

4. N. Kessaris, M. Fogarty, P. Iannarelli, M. Grist, M. Wegner, W. D. Richardson, Competing waves of oligodendrocytes in the forebrain and postnatal elimination of an embryonic lineage. *Nat. Neurosci.* **9**, 173–179 (2006). Medline doi:10.1038/nn1620

5. R. L. Sidman, P. Rakic, Neuronal migration, with special reference to developing human brain: A review. *Brain Res.* **62**, 1–35 (1973). Medline doi:10.1016/0006-8993(73)90617-3

6. B. Nadarajah, J. E. Brunstrom, J. Grutzendler, R. O. Wong, A. L. Pearlman, Two modes of radial migration in early development of the cerebral cortex. *Nat. Neurosci.* **4**, 143–150 (2001). Medline doi:10.1038/83967

7. N. A. O'Rourke, M. E. Dailey, S. J. Smith, S. K. McConnell, Diverse migratory pathways in the developing cerebral cortex. *Science* **258**, 299–302 (1992). Medline doi:10.1126/science.1411527

8. H. Komuro, P. Rakic, Dynamics of granule cell migration: A confocal microscopic study in acute cerebellar slice preparations. *J. Neurosci.* **15**, 1110–1120 (1995). Medline

9. C. Lois, A. Alvarez-Buylla, Long-distance neuronal migration in the adult mammalian brain. *Science* **264**, 1145–1148 (1994). Medline doi:10.1126/science.8178174

10. E. Kokovay, S. Goderie, Y. Wang, S. Lotz, G. Lin, Y. Sun, B. Roysam, Q. Shen, S. Temple, Adult SVZ lineage cells home to and leave the vascular niche via differential responses to SDF1/CXCR4 signaling. *Cell Stem Cell* **7**, 163–173 (2010). Medline doi:10.1016/j.stem.2010.05.019

11. M. Snapyan, M. Lemasson, M. S. Brill, M. Blais, M. Massouh, J. Ninkovic, C. Gravel, F. Berthod, M. Götz, P. A. Barker, A. Parent, A. Saghatelyan, Vasculature guides migrating neuronal precursors in the adult mammalian forebrain via brain-derived neurotrophic factor signaling. *J. Neurosci.* **29**, 4172–4188 (2009). Medline doi:10.1523/JNEUROSCI.4956-08.2009

12. S. A. Goldman, Z. Chen, Perivascular instruction of cell genesis and fate in the adult brain. *Nat. Neurosci.* **14**, 1382–1389 (2011). Medline doi:10.1038/nn.2963

13. H. H. Tsai, H. Li, L. C. Fuentealba, A. V. Molofsky, R. Taveira-Marques, H. Zhuang, A. Tenney, A. T. Murnen, S. P. Fancy, F. Merkle, N. Kessaris, A. Alvarez-Buylla, W. D. Richardson, D. H. Rowitch, Regional astrocyte allocation regulates CNS synaptogenesis and repair. *Science* **337**, 358–362 (2012). Medline doi:10.1126/science.1222381

14. R. J. M. Franklin, C. ffrench-Constant, Remyelination in the CNS: From biology to therapy. *Nat. Rev. Neurosci.* **9**, 839–855 (2008). Medline doi:10.1038/nrn2480

15. M. Finzsch, C. C. Stolt, P. Lommes, M. Wegner, Sox9 and Sox10 influence survival and migration of oligodendrocyte precursors in the spinal cord by regulating PDGF receptor α expression. *Development* **135**, 637–646 (2008). Medline doi:10.1242/dev.010454

16. F. Binamé, D. Sakry, L. Dimou, V. Jolivel, J. Trotter, NG2 regulates directional migration of oligodendrocyte precursor cells via Rho GTPases and polarity complex proteins. *J. Neurosci.* **33**, 10858–10874 (2013). Medline doi:10.1523/JNEUROSCI.5010-12.2013

17. Y. Miyamoto, J. Yamauchi, A. Tanoue, Cdk5 phosphorylation of WAVE2 regulates oligodendrocyte precursor cell migration through nonreceptor tyrosine kinase Fyn. *J. Neurosci.* **28**, 8326–8337 (2008). Medline doi:10.1523/JNEUROSCI.1482-08.2008

18. H. H. Tsai, M. Tessier-Lavigne, R. H. Miller, Netrin 1 mediates spinal cord oligodendrocyte precursor dispersal. *Development* **130**, 2095–2105 (2003). Medline doi:10.1242/dev.00424

19. E. Garcion, A. Faissner, C. ffrench-Constant, Knockout mice reveal a contribution of the extracellular matrix molecule tenascin-C to neural precursor proliferation and migration. *Development* **128**, 2485–2496 (2001). Medline

20. H. H. Tsai, E. Frost, V. To, S. Robinson, C. ffrench-Constant, R. Geertman, R. M. Ransohoff, R. H. Miller, The chemokine receptor CXCR2 controls positioning of oligodendrocyte precursors in developing spinal cord by arresting their migration. *Cell* **110**, 373–383 (2002). Medline doi:10.1016/S0092-8674(02)00838-3

21. A. Baron-Van Evercooren, V. Avellana-Adalid, A. Ben Younes-Chennoufi, A. Gansmuller, B. Nait-Oumesmar, L. Vignais, Cell-cell interactions during the migration of myelin-forming cells transplanted in the demyelinated spinal cord. *Glia* **16**, 147–164 (1996). Medline doi:10.1002/(SICI)1098-1136(199602)16:2<147::AID-GLIA7>3.0.CO;2-0

22. R. Daneman, D. Agalliu, L. Zhou, F. Kuhnert, C. J. Kuo, B. A. Barres, Wnt/β-catenin signaling is required for CNS, but not non-CNS, angiogenesis. *Proc. Natl. Acad. Sci. U.S.A.* **106**, 641–646 (2009). Medline doi:10.1073/pnas.0805165106

23. J. M. Stenman, J. Rajagopal, T. J. Carroll, M. Ishibashi, J. McMahon, A. P. McMahon, Canonical Wnt signaling regulates organ-specific assembly and differentiation of CNS vasculature. *Science* **322**, 1247–1250 (2008). Medline doi:10.1126/science.1164594

24. K. A. Hogan, C. A. Ambler, D. L. Chapman, V. L. Bautch, The neural tube patterns vessels developmentally using the VEGF signaling pathway. *Development* **131**, 1503–1513 (2004). Medline doi:10.1242/dev.01039

25. F. Kuhnert, M. R. Mancuso, A. Shamloo, H. T. Wang, V. Choksi, M. Florek, H. Su, M. Fruttiger, W. L. Young, S. C. Heilshorn, C. J. Kuo, Essential regulation of CNS

angiogenesis by the orphan G protein–coupled receptor GPR124. *Science* **330**, 985–989 (2010). Medline doi:10.1126/science.1196554

26. R. Daneman, L. Zhou, A. A. Kebede, B. A. Barres, Pericytes are required for blood-brain barrier integrity during embryogenesis. *Nature* **468**, 562–566 (2010). Medline doi:10.1038/nature09513

27. S. P. Fancy, S. E. Baranzini, C. Zhao, D. I. Yuk, K. A. Irvine, S. Kaing, N. Sanai, R. J. Franklin, D. H. Rowitch, Dysregulation of the Wnt pathway inhibits timely myelination and remyelination in the mammalian CNS. *Genes Dev.* **23**, 1571–1585 (2009). Medline doi:10.1101/gad.1806309

28. S. P. Fancy, E. P. Harrington, S. E. Baranzini, J. C. Silbereis, L. R. Shiow, T. J. Yuen, E. J. Huang, S. Lomvardas, D. H. Rowitch, Parallel states of pathological Wnt signaling in neonatal brain injury and colon cancer. *Nat. Neurosci.* **17**, 506–512 (2014). Medline doi:10.1038/nn.3676

29. S. P. Fancy, E. P. Harrington, T. J. Yuen, J. C. Silbereis, C. Zhao, S. E. Baranzini, C. C. Bruce, J. J. Otero, E. J. Huang, R. Nusse, R. J. Franklin, D. H. Rowitch, Axin2 as regulatory and therapeutic target in newborn brain injury and remyelination. *Nat. Neurosci.* **14**, 1009–1016 (2011). Medline doi:10.1038/nn.2855

30. T. J. Yuen, J. C. Silbereis, A. Griveau, S. M. Chang, R. Daneman, S. P. Fancy, H. Zahed, E. Maltepe, D. H. Rowitch, Oligodendrocyte-encoded HIF function couples postnatal myelination and white matter angiogenesis. *Cell* **158**, 383–396 (2014). Medline doi:10.1016/j.cell.2014.04.052

31. Y. Choe, S. J. Pleasure, Wnt signaling regulates intermediate precursor production in the postnatal dentate gyrus by regulating CXCR4 expression. *Dev. Neurosci.* **34**, 502–514 (2012). Medline doi:10.1159/000345353

32. G. Banisadr, T. J. Frederick, C. Freitag, D. Ren, H. Jung, S. D. Miller, R. J. Miller, The role of CXCR4 signaling in the migration of transplanted oligodendrocyte progenitors into the cerebral white matter. *Neurobiol. Dis.* **44**, 19–27 (2011). Medline

33. M. Dziembowska, T. N. Tham, P. Lau, S. Vitry, F. Lazarini, M. Dubois-Dalcq, A role for CXCR4 signaling in survival and migration of neural and oligodendrocyte precursors. *Glia* **50**, 258–269 (2005). Medline doi:10.1002/glia.20170

34. B. Vanhollebeke, O. A. Stone, N. Bostaille, C. Cho, Y. Zhou, E. Maquet, A. Gauquier, P. Cabochette, S. Fukuhara, N. Mochizuki, J. Nathans, D. Y. R. Stainier, Tip cell-specific requirement for an atypical Gpr124- and Reck-dependent Wnt/β-catenin pathway during brain angiogenesis. *eLife* **4**, e06489 (2015). doi:10.7554/eLife.06489

35. E. Posokhova, A. Shukla, S. Seaman, S. Volate, M. B. Hilton, B. Wu, H. Morris, D. A. Swing, M. Zhou, E. Zudaire, J. S. Rubin, B. St. Croix, GPR124 functions as a WNT7-specific coactivator of canonical β-catenin signaling. *Cell Rep.* **10**, 123–130 (2015). Medline doi:10.1016/j.celrep.2014.12.020

36. M. D. Tallquist, W. J. French, P. Soriano, Additive effects of PDGF receptor β signaling pathways in vascular smooth muscle cell development. *PLOS Biol.* **1**, e52 (2003). Medline doi:10.1371/journal.pbio.0000052

37. U. Schüller, V. M. Heine, J. Mao, A. T. Kho, A. K. Dillon, Y. G. Han, E. Huillard, T. Sun, A. H. Ligon, Y. Qian, Q. Ma, A. Alvarez-Buylla, A. P. McMahon, D. H. Rowitch, K. L. Ligon, Acquisition of granule neuron precursor identity is a critical determinant of progenitor cell competence to form Shh-induced medulloblastoma. *Cancer Cell* **14**, 123–134 (2008). Medline doi:10.1016/j.ccr.2008.07.005

38. E. C. Robanus-Maandag, P. J. Koelink, C. Breukel, D. C. Salvatori, S. C. Jagmohan-Changur, C. A. Bosch, H. W. Verspaget, P. Devilee, R. Fodde, R. Smits, A new conditional Apc-mutant mouse model for colorectal cancer. *Carcinogenesis* **31**, 946–952 (2010). Medline doi:10.1093/carcin/bgq046

39. Y. R. Zou, A. H. Kottmann, M. Kuroda, I. Taniuchi, D. R. Littman, Function of the chemokine receptor CXCR4 in haematopoiesis and in cerebellar development. *Nature* **393**, 595–599 (1998). Medline doi:10.1038/31269

40. N. Tekki-Kessaris, R. Woodruff, A. C. Hall, W. Gaffield, S. Kimura, C. D. Stiles, D. H. Rowitch, W. D. Richardson, Hedgehog-dependent oligodendrocyte lineage specification in the telencephalon. *Development* **128**, 2545–2554 (2001). Medline